Sub-microradian Pointing for Deep Space Optical Telecommunications Network

Gerry G. Ortiz, Shinhak Lee, and James W. Alexander

Jet Propulsion Laboratory, California Institute of Technology
4800 Oak Grove Drive, MS 161-135 Pasadena, CA 91109

ABSTRACT

NASA/JPL has been developing technologies for a novel and unified approach to point a laser beam from deep space with sub-micro-radian precision for optical communication systems. The approach is based on using high bandwidth inertial sensors to compensate for jitter excursions caused by spacecraft vibrations. This use of high bandwidth inertial sensors enables the implementation of laser communication links anywhere within the solar system (and even beyond).

A widely accepted scheme for accomplishing the detection, tracking, and pointing function (required in free-space optical communications) is to split a fraction of a received uplink beacon signal and direct it onto a focal plane array (FPA) detector. The motion of the focal spot on the FPA is tracked to accurately point the downlink data signal to the Earth receiving station. For deep space links, the historical approach to compensate for spacecraft vibrations and dead-band excursions has been to close a high-bandwidth pointing-control-loop using optical-tracking (> 500 Hz). But, this method required the use of a separate uplink beacon (laser or Earth image). However, studies have shown that using these optical-tracking references become limited in tracking bandwidth in deep space applications, because of the small amount of signal reaching the spacecraft. Our recent analysis and simulations indicate that, by augmenting the current architecture (celestial optical tracking) through the use of high rate inertial sensors (gyros, accelerometers, rate sensors), the tracking and pointing performance will be improved to the sub-micro-radian level.

Analogous to an attitude and control subsystem, the spacecraft motion is measured using the gyros, and this measurement is used to correct instrument pointing. Optical updates are then made infrequently to correct for the low frequency inertial sensor drift. Since optical measurements are no longer needed at the rate required to close the pointing compensation loop, such a scheme allows for a significant reduction of the required tracking update rate. Furthermore, this technique enables the use of dimmer stars (and/or a dim uplink laser). Therefore, combined with a low rate, high accuracy optical tracker, these inertial sensors can be successfully used to compensate for jitter, to close the control loop and to point to a receiving station with sub-micro-radian accuracy. This presentation will cover innovative hardware, algorithms, architectures, techniques and recent laboratory results that are applicable to all deep space optical communication links, such as the Mars Telecommunication Network to future interstellar missions.

Key Words: Deep space optical communications, tracking, pointing, inertial sensor, Mars Network.

1 INTRODUCTION

NASA has been developing communication systems that enable affordable virtual presence throughout the solar system by increasing volume and timeliness of space data transfer directly to users while minimizing the cost and the impact of communications subsystems on future spacecraft. One highly promising technology to achieve this goal is free-space optical communications. But, in order to enable this technology, an acquisition, tracking and pointing (ATP) architecture that is independent of range (to receiver system) needs to be developed. Furthermore, pointing error analysis has shown that S/C vibration

is the dominant contributor to mis-pointing[1], Therefore, the ATP functions have to be demonstrated to clearly and effectively compensate for spacecraft (S/C) jitter in a simulated vibration environment.

The effect of spacecraft vibration upon the pointed optical signal is graphically shown in Figure 1. There is a large slow motion due to S/C dead-band excursion and a fast jitter excursion due to vibrations. Generally two mechanisms are used to compensate for these motions. One is to determine the known motion and the second is to use fast rate sampling. The known motion is typically obtained by sampling a focal plane array (FPA) that has the receiver laser beacon imaged onto it. This can be done at a low sampling rate since the dead-band excursion is typically no greater than 30 Hz. To compensate for jitter, the FPA sampling rate is typically increased to 10 times[2] the expected vibration signal (e.g. 2-3 kHz for vibration spectra content to 300 Hz). But, for deep-space applications this requires a very strong beacon (i.e. short exposure times) and eliminates the possibility of using other sources for the beacon signal (e.g. stars, extended earth-image). In order to alleviate this difficulty and to enhance the utility of the legacy architecture[3], a high bandwidth inertial sensor has been introduced to provide compensation for S/C jitter[4]. Inertial sensors are available that can be sampled at very high rates (up to 10 kHz). Figure 1 demonstrates qualitatively that with optical compensation only there will be some residual error. By introducing an inertial sensor into the control loop to provide compensation the RMS error and worst case effect of platform vibration is reduced.

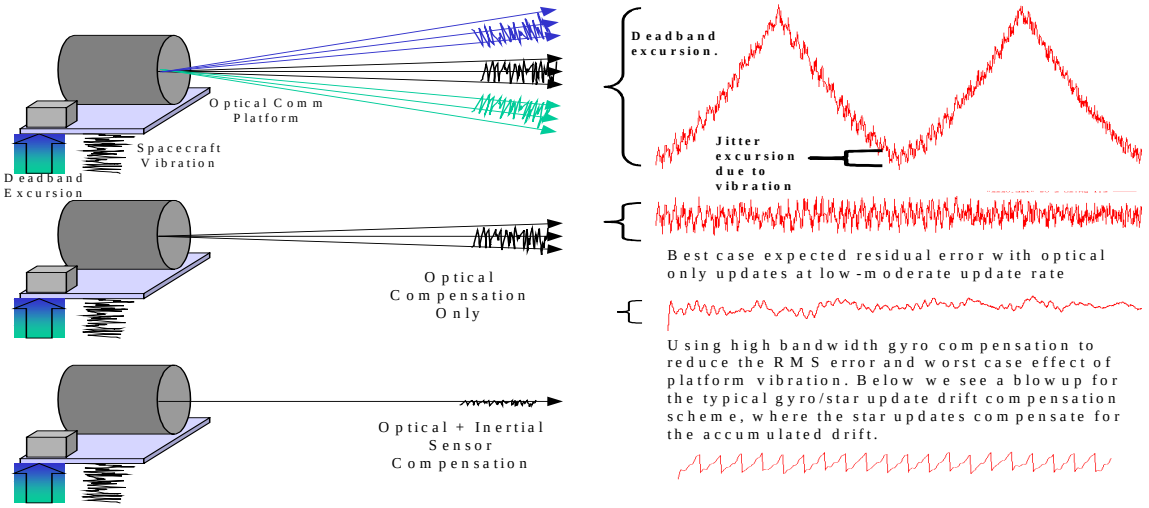

Figure 1. Effect of spacecraft dead-banding and vibration on pointed optical signal.

This enhancement to the single-FPA ATP architecture has numerous advantages. It is independent of range, it can use natural and artificial beacons, it can have a steady reference update rate, and it only requires a single high precision FPA (without requiring a high rate frame transfer). This new architecture is shown in Figure 2. Whereas the legacy architecture [3] depended on a single fast control loop, this enhanced architecture utilizes a slow control loop to compensate for known motion and a fast control loop to compensate for S/C vibration.

Progress in the development of the ATP Subsystem for an Optical Telecommunications Network is presented in this article. Section 2 presents the methods and algorithms for accelerometer-assisted tracking. Section 3 discusses recent progress in the development of innovative hardware and components for deep-space ATP systems. In particular, the following areas will be covered, i) ATP testbed, ii) recent advances in fine pointing control for deep space, iii) an advanced CCD camera and iv) the specifications and performance of a vibration platform testbed (VPT) specifically developed for testing ATP concepts for deep space. Furthermore, section 4 presents the latest laboratory functional validation of using this new architecture with accelerometers to assist in beacon tracking. This is shown by: i) validation of the

algorithms used to estimate displacement, ii) demonstrating that achievable performance meets deep space requirements, and iii) tracking beacon under vibration.

2 CONCEPT AND ANALYSIS

The most critical tracking parameter to achieve sub-microradian pointing while undergoing spacecraft vibration is the tracking update rate. Since the degree of suppression of spacecraft vibration is proportional to the ability to measure it, faster measurements will improve the pointing. Current tracking systems rely on optical beacon sources such as ground based laser beacon, extended sources (such as Sun-illuminated Earth or Moon), and stars. However, for deep space ranges, the intensity of these beacon sources is not sufficient to support the required optical tracking rate (typically a few kilohertz). However, the tracking rate can be increased by employing inertial sensors, which can propagate the line of sight between optical measurements, command the pointing mechanism, compensating for the spacecraft vibrations, effectively increasing the tracking rate. In this section, we will present the concept of accelerometer-assisted tracking and error analysis. Progress made on its implementation is presented is section 4.

2.1 Accelerometer-assisted Tracking

The architecture of the proposed tracking and pointing subsystem employs two tracking loops, one for low frequency measurements through optical tracking (in some sense, a correction update) and high frequency measurements through inertial tracking. This architecture is depicted in Figure 2. In order to use linear accelerometer pairs to measure angular displacements, either software or hardware implementation is required to perform double integration. Previously, both hardware and software implementation for double integration were attempted. However, hardware implementations (analog double integrator) were reported to have many significant problems whereas the proposed software implementation was limited to displacement signals with zero mean value due to the application of high pass filters[5,6]. Our approach is to use the trapezoidal rule, a well-known numerical integration method, along with a least squares fit on a collection of accelerometer measurements and reference optical measurements. This allows the effects of acceleration bias, initial velocity error, and scale factor error to be minimized. The process of estimating single-axis angular displacement from linear accelerations is given in the following (two axes will require a minimum of three linear accelerometers).

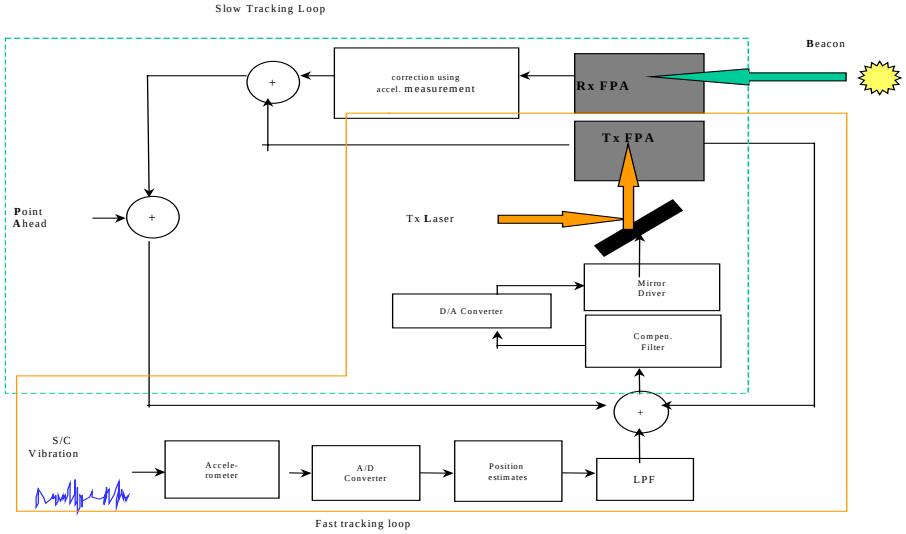

Figure 2. The architecture, highlighting the slow and fast control loops.

A pair of parallel mounted accelerometers A_1 and A_2 are shown in Figure 3a. The angle, θ, can be estimated from the individual readings of accelerometers, A_1 and A_2, after converting the accelerations into linear displacements, d_1 and d_2 with the small angle assumption, $\theta = (d_1 - d_2)/ l$. Since *l*, the separation, is a known measurable constant, θ is determined with the precision of A_1 and A_2. Angular displacements on two axis (α, β) can be obtained using three accelerometers as shown in Figure 3b. Three accelerometers are placed on the y-z plane. Assume acceleration is in x-direction, then displacement estimation using accelerations from B and C gives an angular displacement (α) on x-y plane. Using A and the mean of B and C gives an angular displacement (β) on the x-z plane.

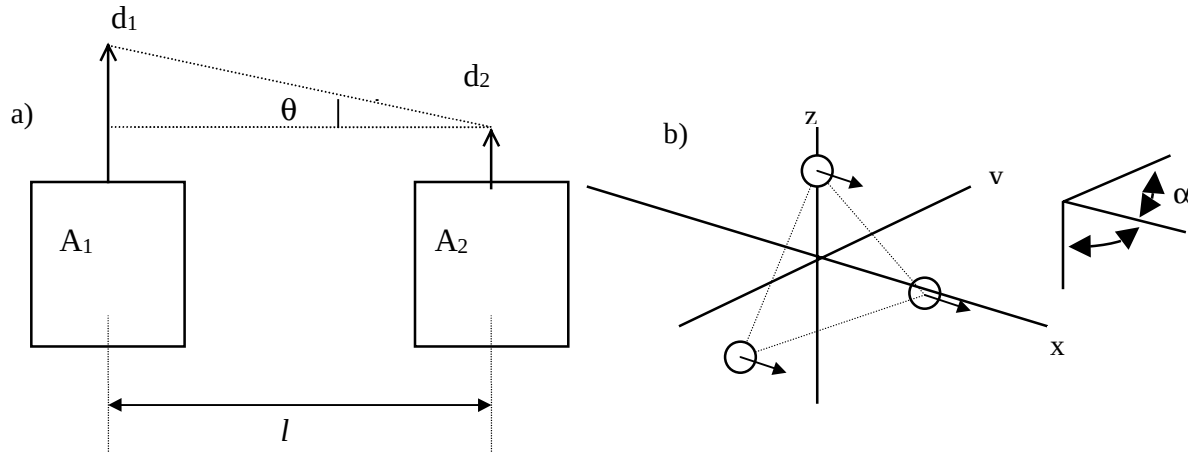

Figure 3a) A pair of linear accelerometers arranged to estimate a single axis angular displacement. 3b) Triangular arrangement of accelerometers to estimate two-axis angular displacements.

2.2 Error Analysis

There are two types of errors caused by the accelerometers that affect displacement estimation errors: accelerometer electronic noise and frequency response error. Electronic noise is the wide bandwidth random noise. Electronic noise is the primary error factor for displacement estimation while the frequency response error is the static error that is a function of frequency. The frequency response error is rather small and calibration can reduce it down to 0.5% for AlliedSignal QA3000 accelerometers. Therefore, we will focus on electronic noise for performance estimation hereafter. In order to estimate the displacement error from accelerometer noise, a displacement estimation equation in terms of acceleration needs to be derived. This derivation has been reported in [5].

The position estimation error (1 sigma value) using QA-3000 accelerometer noise of 76 μg (10~500 Hz) and sampling rates of 2 kHz and 5 kHz are plotted in Figure 4 for an integration period up to 100 msec assuming accelerometer separation of 30 cm. From this plot, requirements on accelerometer noise can be deduced. For sub-microradian pointing, angular displacement estimation error should not exceed 0.16 μrad (0.071μrad*1μrad/0.45μrad) if we take previous mission studies such as Europa mission study where 0.071μrad was allocated to the displacement estimation error for the total RMS tracking error of 0.45 μrad[7]. This translates to linear displacement error of 0.034 μm that corresponds to the maximum integration period of 0.03 second or optical tracking rate of 33 Hz for 5 kHz sampling. Since the angular displacement error is directly proportional to the accelerometer noise, different optical tracking rate will result in variations from 76 μg. Table 1 shows the requirements on accelerometer noise when various optical tracking rates are used assuming 5 kHz accelerometer sampling.

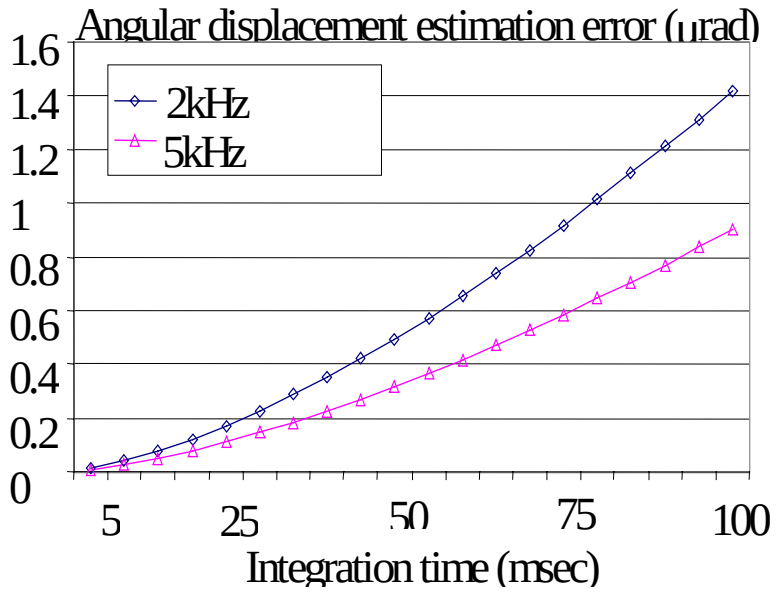

Figure 4. Angular displacement estimation error vs. integration period assuming 0.3m separation of two accelerometers. Acceleration measurement error of 76μg was used for two sampling frequencies (2kHz and 5kHz). Notice that higher sampling frequency gives better performance.

rate	10Hz	20Hz	30Hz	50Hz	100Hz
noise	13μg	38μg	69μg	152μg	428μg

Table 1. Requirements on accelerometer noise for various optical tracking rates for pointing error of 0.16 μrad due to accelerometer.

We presented the concept and error analysis of accelerometer-assisted tracking. This inertial sensor (accelerometer) tracking approach promises the improvements of the performance of ATP subsystem while using the low intensity beacon sources such as uplink laser, stars, and Sun-illuminated Earth images as optical references. The primary challenge in using accelerometers to achieve the desired tracking performance is the minimization of the total random noise in acceleration measurements. Future work includes upgrades of hardware to lower the random noise. For flight implementations, there are other error sources that probably need to be estimated. One of the examples includes accelerometer-to-accelerometer distance that will likely vary with temperature and disturbances.

3 ATP SYSTEM DEVELOPMENT

This section describes improvements made to the existing implementation of the JPL patented Optical Communications Demonstrator Acquisition and Fine Tracking System. A laboratory test bed has been developed for the purpose of analyzing, implementing, and testing a high bandwidth, precision pointing and tracking system for free-space optical communications. The test bed system has been developed to aid in the implementation of complex algorithms to enable Free-Space optical Communications for Deep-Space scenarios. Furthermore, this section will present progress in pointing control, a new CCD based high-frame rate camera and a vibration platform to be used for validation of the pointing technology.

The test bed system allows for the implementation of Acquisition, Tracking, and Pointing functions in an effort to obtain an understanding of the discrete components and how each component affects the overall system performance. The integrated system is based on the JPL patented Optical Communications Demonstrator Architecture [3]. The architecture contains a Fine Steering Mechanism, Focal Plane Array Detector, Tracking Processor & Control Electronics, Host Processor for User interfacing and control and

two Helium Neon visible lasers. Characterization and validation of the fine pointing control subsystem is facilitated by the test bed and is therefore the focus of this paper. Results presented demonstrate improvement in the rejection bandwidth of the fine pointing control system by upgrading the fine steering mirror with a larger open loop control bandwidth than the legacy fine steering mirror. Improvement is demonstrated from the previous fine steering mirror rejection bandwidth of 60 Hz to 70 Hz after reducing the system sample rate to 1 kHz (from 2 kHz).

3.1 ATP Testbed

The ATP test bed optical setup is comprised of four optical channels. These are the transmit beam channel, the beacon channel, the focal plane array (FPA) channel and a public demo channel. The transmit channel contains the down link laser beam (simulated here with a red HeNe), which is pointed towards the ground receiver with the fine-steering mirror. Part of the transmit signal is split in a beam splitter and imaged onto the FPA using the optics in the FPA channel. The beacon channel collects the ground laser beacon (simulated here with a green HeNe). This channel also contains a steering mirror for simulating orbital motion, and ground beacon jitter. The beacon channel is combined with the transmit channel using a beam splitter in order to image it onto the FPA. Both beacon and transmit channels are projected onto a target using the public demo channel. This channel allows for ease of visualization of bean motion on the FPA. As a test bed this setup was designed with control parameters to enable characterization of the different components that comprise the ATP system. The testbed allows control of the spot sizes on the FPA, varying from 130 μm to 60 μm. Also, neutral density (ND) filters have been

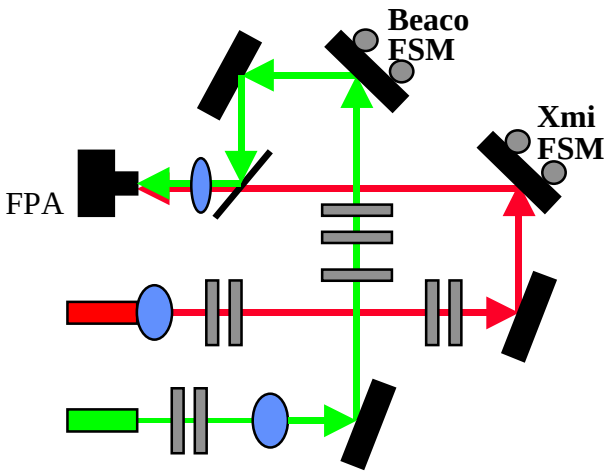

Figure 5a) ATP Test Bed

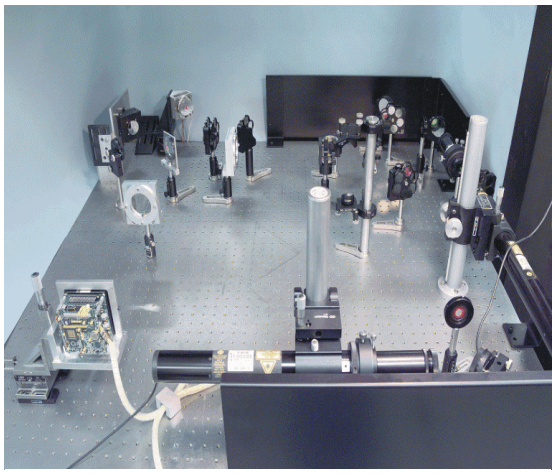

Figure 5b) Photograph of the ATP Optical

included to control the intensity of the spots on the FPA. The ND filters enable testing of centroid algorithms and characterization of FPAs. The optical setup includes alignment mirrors that facilitate the ability to replace existing components with upgrade components for the purpose of characterization (eg. replacing the FSM or FPA).

The tracking system hardware consists of a Host PC, a Texas Instruments TMS320C40 Digital Signal Processor (C40), Tracking Processor Electronics, a modified Dalsa CCD, and Left Hand Design's Fast Steering Mirror (FSM), henceforth denoted as FO35. Real-time control of the FSM is implemented in the C40 software. The Host PC utilizes a Graphical User Interface to enable user input and data gathering during real-time operation. Communication between the C40 and the Host PC is accomplished via an ISA standard interface to pass data and control parameters from the Host PC to the C40. A Dalsa CCD Camera that has been modified to facilitate the extraction of sub-windowed images at high frames, minimum 1000 frames per second for these experiments constitutes the FPA.

3.2 Fine Pointing Control

The C40 runs the acquisition, tracking, and fine pointing control software. The acquisition algorithm implemented extracts a single 10x10-pixel window, one full frame per window, from the FPA in search of a valid beacon centroid signal. The search is implemented by partitioning the 128x128-pixel area into 10x10 sub-windows. A centroid calculation is performed on each sub-window. Once a valid beacon has been located[8], the tracking software commences to close the control loop of the steering mirror based on the centroid data, see figure 4. A software state machine executes the transition from acquisition mode to tracking mode. The FSM control loop is optically closed by comparing the beacon position with the transmit laser position with an optical offset added to avoid overlap between the two laser spots. The difference between the two laser spot locations is then used as the error signal into the control loop. The amount of error signal injected into the control loop is initially limited due to the inability of the image tracking software to track laser spots at high angular rates. Once the error signal is at a low level, the full error is then injected into the control loop. The tracking software then attempts to stabilize the line of sight for the transmit laser using optical feedback, as shown if figure 6.

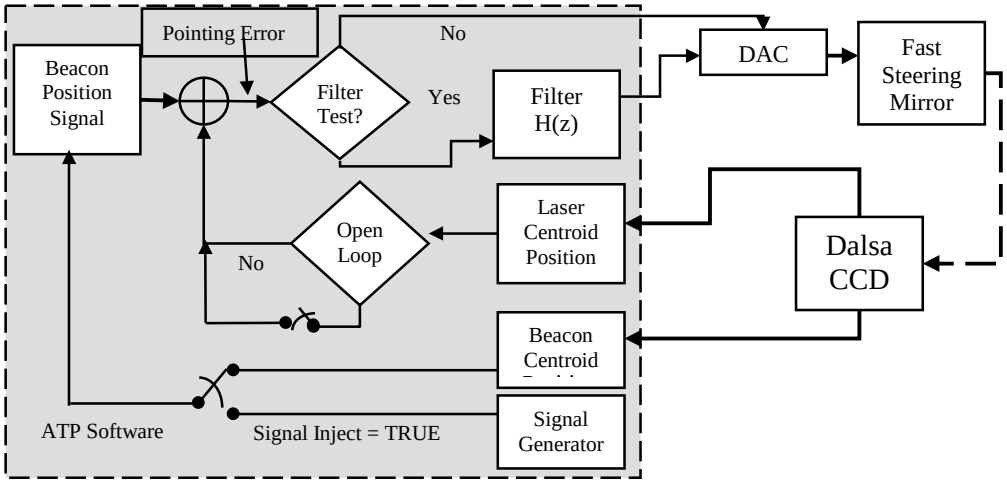

Figure 6 Software Description.

Real-time operation of the fine pointing control loop is defined by five steps. The timing and execution of each step is critical for optical tracking and pointing control. The amount of time delay induced by digital processing of data used by the feed back path can significantly reduce the performance achievable[9]. Previous experiments demonstrated a 3-sample delay in the optical tracking system digital control loop[10]. The majority of the system delay comes from the CCD, which acts as the feedback path.

Close loop performance was verified by injecting digital sine waves at discrete frequencies into the input of the fine pointing control loop. The data was processed to determine the close loop response of each mirrors' axis. The rejection bandwidth was predicted using Matlab and verified to be approximately 70 Hz for each FO-35 axis, see figure 7.

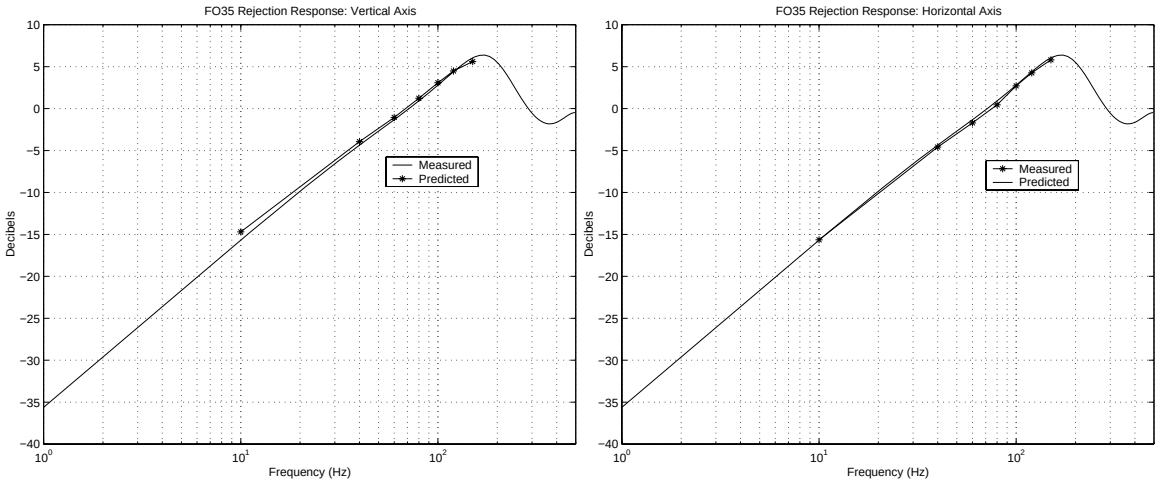

Figure 7. FO-35 Rejection response, vertical and horizontal axis.

In conclusion the close loop and rejection bandwidth have been improved from previous experiments using new FSMs. The improvements are apparent even after reducing the control loop sample rate by a factor of two. Time delay limitations previously measured, have been identified in the digital control loop implementation. Limitations in the control loop and rejection bandwidth are attributed to the limited processing bandwidth that is characteristic to the implemented hardware and software architecture. The processing bandwidth of the ATP system limited the experiments to 1 kHz FSM command rates. The next steps to improve the implemented tracking loop are to upgrade the FPA with a faster CCD sensor, migrate the existing fine pointing control software to a faster processing platform, and implement inertial sensors to alleviate the need for high beacon update rates. Development of a faster FPA is addressed in the next section.

3.3 High Frame Rate CCD Camera with Region-of-Interest Capability

This section presents the design and preliminary results of a custom high-speed CCD camera utilizing a Texas Instruments TC237 CCD imager chip with sub-frame window read out. The camera interfaces to a C40 digital signal processor (DSP), which is used to issue commands and read images from the camera. The camera design consists of a two-card set including the CCD imager card and the focal plane array (FPA) interface card. The CCD imager card contains the level translator and buffer circuitry for the CCD strobe lines, the TC237 CCD imager chip and a pair of analog signal processor chips, each with a 10-bit analog-to-digital converter. The analog signal processor is a TLV987 with correlated double sampling (CDS) and serial programming capability to set amplifier gain, pixel bias level and background level illumination to name a few. The second card contains a pair of field programmable gate arrays (FPGA) used to interface the CCD imager card to the C40. Further design details and results have been presented elsewhere[11]. The goal of this camera development is to provide a high-quality, high-speed camera as part of the tracking apparatus for a free-space optical communications terminal. Preliminary data suggests frame rates of 6 kHz for 8x8 sub-windows in the current testbed with 7-bit pixel resolution. Refinements in camera and testbed operation target performance goals of 17 kHz for 8x8 sub-windows with 10-bit pixel resolution.

The TC237 is a CCD imager with an image area of 680 pixels per line and 500 lines[12]. The active image area of the CCD is 658 pixels per line and 496 lines and contains all exposed pixels during scene capture. There are additionally 22 pixels per line and four additional lines of dark pixels, which make up the remainder of the image area and are used for background level calibration. The TLV987 is an analog signal processor with a 10-bit analog-to-digital converter (ADC) at the output. It has a total of nine registers for customizing device operation. With the exception of the gain block, the TLV987 is used in

the default mode as described in [13]. Preliminary test results presented below used a gain of approximately 6 dB for the gain block.

Read out of a sub-window consists of three fundamental operations. They include a refresh operation, scrolling through the image until the sub-window is reached and reading the pixels which are in the sub-window. The time required to read out a sub-window is defined as the sum of the refresh time, the scroll time and the window read time.

Table 1 displays calculated window frame rates for two sub-windows within the selected regions of the TC237 FOV. The FOV is defined to include both imaging pixels and covered pixels, used for black level calibration, and is 680 pixels per line by 500 lines per frame [12]. The TC237 is assumed to operate at rates of 10 MHz or 20 MHz for both serial pixel output rate and line transfer rate during a refresh operation. The pixel readout rate from the FIFO buffer to the C40 is approximately 4 MHz for the legacy testbed. The operating scenario is to extract two 8x8 sub-windows within a 128x128 region of the CCD FOV (columns 2 & 4) and two 8x8 sub-windows within a 256x256 region of the CCD FOV (columns 3 & 5). The 128x128 and 256x256 regions include the first line and column of pixels of the CCD FOV. Pixel read out begins with the first line and first column of the TC237 FOV.

Readout Operation	**128x128 10MHz pixel rate**	**256x256 10MHz pixel rate**	**128x128 20 MHz pixel rate**	**256x256 20 MHz pixel rate**
Refresh Time (μS)	50	50	25	25
First Window Scroll Time (μS)	52	116	26	58
Inter-Window Scroll Time (μS)	2.5	2.5	1.3	1.3
Row Read Time First Window (μS)	13.8	26.6	7.9	14.3
Window Read time First Window (μS)	110.4	212.8	63.2	114.4
Row Read Time Second Window (μS)	13.8	26.6	7.9	14.3
Window Read Time Second Window (μS)	110.4	212.8	63.2	114.4
Frame time (μS)	325.3	594.1	178.7	313.1
Frames per Second	3075	1683	5596	3194

Table 2. TC237 readout times for two sub-windows.

In this table, the refresh time is the time needed to transfer all 500 lines from the image area to the storage area. The scroll time is the time required to shift out unwanted lines from the CCD storage area until the first line of the first sub-window is reached. The inter-window scroll time is the time needed to scroll through lines between the last line of the first sub-window and the first line of the second sub-window. The row and window read times are the times required to read out a single row and all rows of a sub-window respectively. The frame rate is the reciprocal of the sum of the frame, scroll and window read times. Preliminary results indicate that the camera can read 8x8 sub-windows at a maximum frame rate of 6 kHz. This rate is for 10 MHz pixel and line transfer rates. The 8x8 sub-window is positioned in the second line and column of the CCD FOV.

Figure 8 shows a 128x128 image taken with the CCD camera and the histogram for this image. The horizontal axis of the histogram represents pixel intensity with an 8-bit dynamic range and the vertical axis is the number of pixels with a particular intensity value. This image was taken with an approximate

gain of two in the TLV987 and a 10-msec integration time. The integration time was defined by setting the frame rate to 100 Hz. This image was taken to get a basic assessment of camera operation. As can be seen from this image, the pixel intensities are distributed over half of the 8-bit dynamic range. From this image, we see that the ADC dynamic range is too large for the given image intensity and gain setting in the TLV987. A better match to the ADC dynamic range is achievable by increasing the gain setting in the TLV987. More work is needed to configure the TLV987 before quantitative characterization of camera images can be done. A signal versus time plot, for a TLV987 gain of two, led to the estimate of about 400 signal electrons per digital number (DN), based on detector full well capacity. The TLV987 gain was set too low for this plot; near-term modifications will be made to allow changing the gain, and then characterizing the detector noise and linearity, along with the spatial uniformity and residual image analysis.

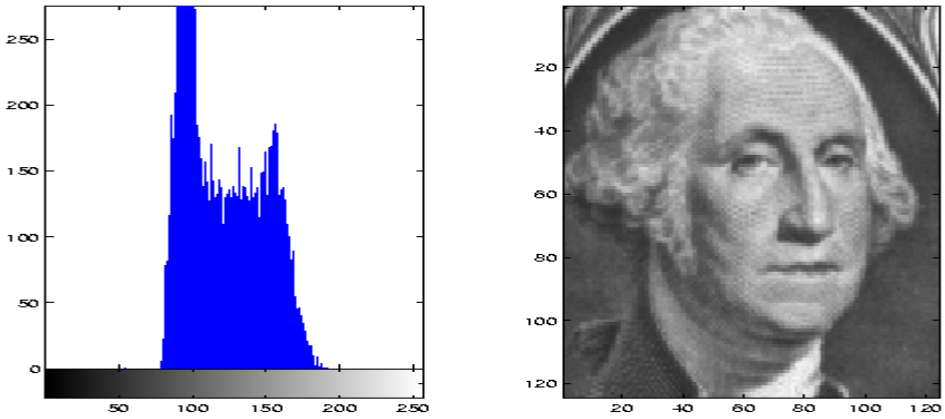

Figure 8. 128x128 Image from CCD Camera.

This section presented a camera design based on the Texas Instruments TC237 CCD imager chip. The motivation in designing a custom camera is to achieve sub-window imaging capability for frame rates of several kilohertz with 10-bits of resolution per pixel as part of the tracking apparatus for a free-space optical communications link. Preliminary results for the camera exhibit a frame rate up to 6 kHz for a single 8x8 sub-window within the FOV of the CCD imager chip with 7-bits of resolution per pixel. These results are for release 1.0 of the camera, which was designed to interface with a legacy testbed for evaluation purposes of the camera. Future work involves characterization of the optical qualities of the camera. The TLV987 parameters, including bias calibration and black-level control to name a few, are currently set to the device defaults with the gain of the device being hardwired to a single setting. In order to characterize the optical qualities of the camera, additional logic is needed to program the TLV987 registers. Release 2.0 of the camera will aim to increase the pixel rate from the camera to 30 mega-pixels per second and increase the pixel dynamic range to 10 bits. The increase in pixel rate will be achieved by increasing the camera system clock to 15 MHz and utilizing both pixel output ports of the TC237 CCD. Improvements in the pixel dynamic range require additional adjustments to the CCD control signals from the FPA interface card. Such adjustments may include modifications to both the sequence and timing of the TC237 control signals to improve clearing and transfer of charge within the CCD. This camera development provides a necessary component for an optical communications terminal. The outcome of this work will determine the limitations of this camera design, the suitability of the TC237 imager chip for optical tracking applications and define how best to operate the camera for different scenarios. It will provide a road map to address any deficiencies found with this implementation and suggest possible avenues for future implementations.

3.4 Vibration Platform Testbed

The Vibration Platform Testbed (VPT) is being developed as a low cost, single axis vibration platform to assist with the development and characterization of acquisition, tracking and pointing (ATP) systems for deep space optical communication at JPL. To accurately point at the earth, an optical communication system for a deep space mission must possess the capability to correct for jitter induced by the spacecraft. Ideally, the VPT will subject the optical communication system under test to a vibration spectrum that is likely to be encountered while onboard a spacecraft. The goal of the VPT is to provide several cases of single axis motion with a vibration spectrum out to 150 Hz and a maximum angular displacement of 200 μrad.

The VPT system consists of a 61 cm by 61 cm optical breadboard, mounted on a shaft/pillow block assembly that is used as a pivot, and driven by a piezo-electric actuator (PZT). The breadboard is a Melles Griot UltraPerformance Series (product number 07 OBC 005) chosen for the high compliance specifications. The shaft/pillow block assembly is mounted directly under the centerline of the breadboard. The PZT, manufactured by Polytec PI (model P-841.40), is located below one end of the breadboard and provides the motion for the system. As the PZT should only operate in either a push or a pull mode, but not both, it is highly advisable not to mount the breadboard directly to the PZT. A "ball bearing tip" was manufactured to serve as the contact point between the PZT and the breadboard. Since it was not possible to directly mount the breadboard to the PZT, one expansion spring is located at each corner to provide the force necessary to keep the breadboard in contact with the PZT. The VPT assembly is shown in Figure 9. The CCD camera is seen at the lower portion of the figure. The fine steering mirror used to point the beam is located directly across from the CCD and accelerometer is seen towards the front of the table. Several optics used to focus the beam and split the paths. The displacement is provided by a PZT actuator which can provide motion out to approximately 150 Hz with a 3 dB bandwidth. The maximum angular displacement at this frequency is approximately 100 μrad. At lower frequencies the VPT can provide 200 μrad of angular displacement. By interchanging the PZT actuator with another model, it is possible to obtain a larger range of motion, higher resolution, higher bandwidth, or greater load handling capability.

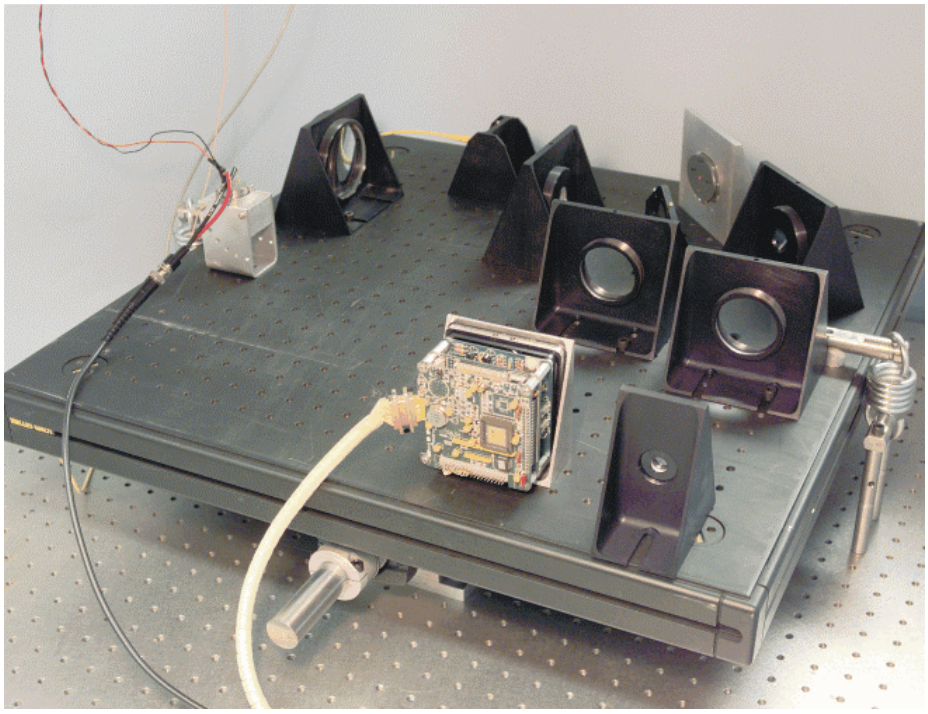

Figure 9. Vibration Platform Testbed with acquisition, tracking and pointing system.

4 Laboratory Validation of Accelerometer-Assisted Beacon Tracking

The steps completed to achieve inertial-sensor based ATP were algorithm development, theoretical analysis, simulation, lab validation of the algorithm and concept demonstration[14]. In order to demonstrate the concept an accelerometer was integrated into the control loop, the algorithms were implemented into the legacy ATP system, and pointing control was demonstrated using a fast steering mirror (FSM).

Three algorithms were developed. These were the double integration position estimator, acceleration bias estimator, and the initial velocity estimator[15]. The accelerometer scale factor is currently estimated using specific values and offline calibrations. Figure 10a shows a sampled acceleration using the QA-3000 from Allied Signal. The acceleration signal was obtained by mounting the accelerometer on JPL's Vibration Platform Testbed[16]. A piezo-electric linear actuator provides the motion for this testbed. The sampled acceleration was analytically processed to obtain an estimate of the displacement using the three algorithms. Figure 10b compares the estimated displacement to the true value. The true value was obtained using a strain-gauge displacement sensor that is built-in to the linear actuator. Very good agreement is obtained thereby validating the algorithms developed.

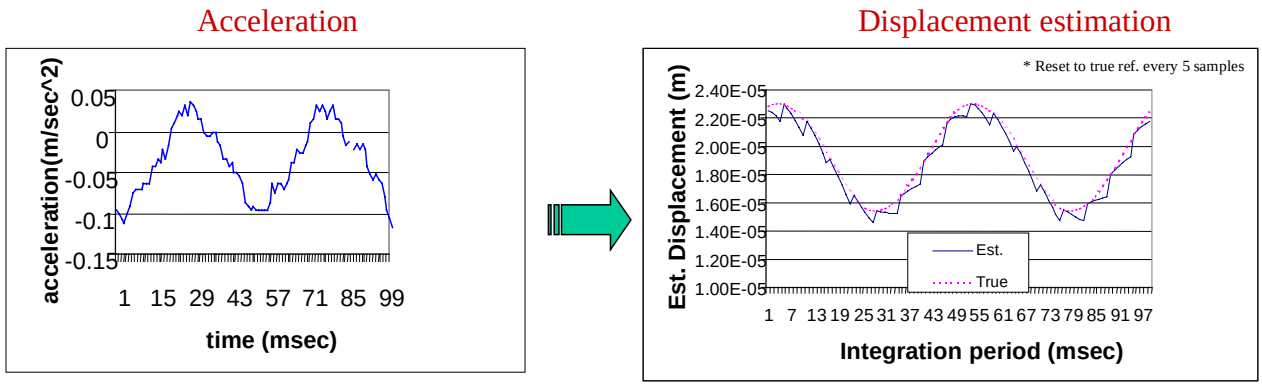

Figure 10a) Sampled acceleration from vibration platform. **10b)** Good agreement demonstrated between estimated displacement and true displacement.

Simulation of the performance achievable with accelerometer-assisted tracking is shown in Figure 11. This step was performed in order to confirm that the errors propagated from accelerometer and algorithms were within the allocated budget to meet deep space pointing requirements. For this simulation the noise was taken as a random, one sigma value of 7.6 μg from 0-10 Hz and 76 μg from 10 to 1000 Hz, as per vendor specs. The displacement algorithm is based on the trapezoidal rule. A Mars link with less than 1 micro-radian pointing error requires that the displacement estimation error be less than 0.2 microradians [1]. Figure 11 demonstrates the dependence of the displacement error on the integration period and the sampling rate. The error demonstrates a t-squared dependence with integration time. As highlighted in the figure, in order to maintain within the allocated error, the fast control loop (running at 1 kHz) will need to be updated every 43 Hz with the optical tracking reference signal in order to reset for the accumulated drift. Both of these rates are readily achievable with today's technology. By operating the optical reference signal at such low update rates, it allows for long integration times and therefore enables the use of stars and extended earth-image tracking. Increasing the sampling rate of the fast control loop will decrease the accumulated drift[17], thereby allowing even longer integration times. Furthermore, when beacon signal is stronger, the reference update rate can be increased to reduce the error and thereby provide more margin to the communications link.

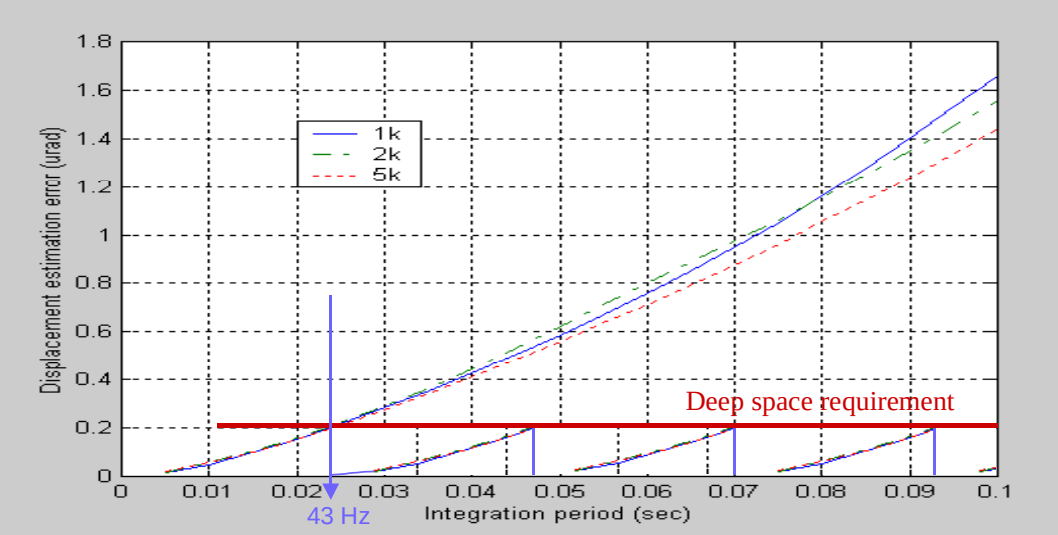

Figure 11. Displacement estimation error dependence on integration period and accelerometer sampling rate.

A simple experiment was performed to validate the algorithms and to gauge the performance achievable with our sampling equipment. The experiment consisted of mounting the accelerometer on the VPT, introducing sinusoidal vibrations at various frequencies, sampling the accelerometer, and having the algorithms compute the estimated displacement. The resulting experimental displacement estimation error is shown in Figure 12 compared to the simulation results. As can be seen very good agreement is obtained. The overall estimation error is larger in this experiment over the simulated results of figure 11. A large component of this increase is believed to be caused by the high level of ambient noise in the laboratory. A base noise of 300 μg's was measured which is 5 times larger than the sensitivity of the accelerometer.

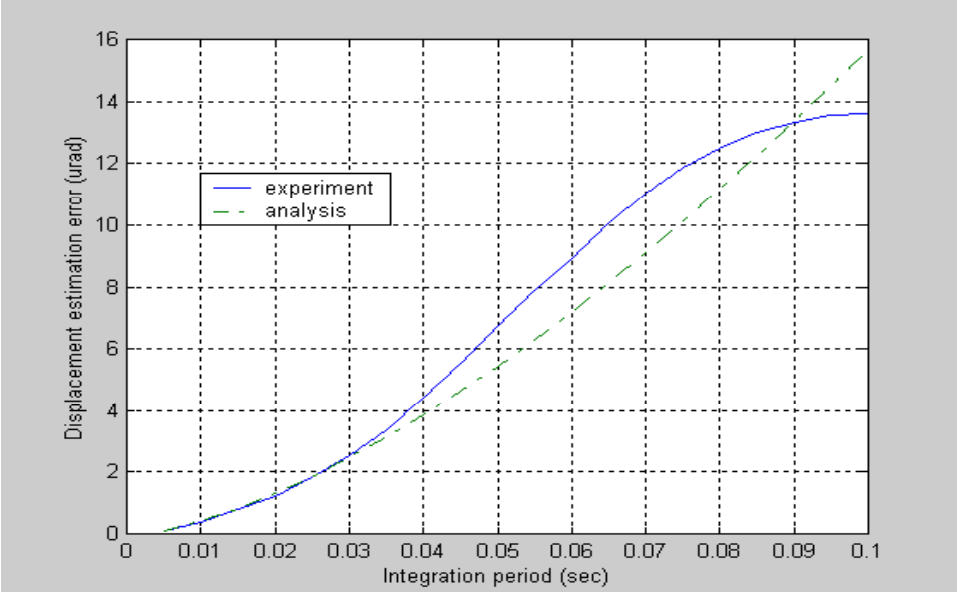

Figure 12. Experimental displacement estimation error.

Accelerometer-assisted beacon tracking was functionally demonstrated using the laboratory set-up depicted in Figure 131. The set-up is comprised of a slow-rate control loop ('optical-tracking') interlaced with a fast-rate control loop ('accelerometer-tracking'). The beacon laser and accelerometer are mounted on the vibration platform driven by the piezo-electric linear actuator. The beacon beam and transmit laser are imaged onto a custom high-rate 128x128 CCD[18] Dalsa camera. The pointing mechanism is an FO-35 fine-steering mechanism (FSM) from Left-Hand Design Corporation.

In the functional demonstration, the fast-rate control loop samples the accelerometer at a 1 kHz rate, estimates the new position, and updates the command to the FSM. This command to the FSM is interlaced every 5th frame with updates from the slow-rate control loop (optical reference update). This reference is obtained by sampling the CCD (at effectively 200 Hz), computing the centroid of the beacon location and updating the command to the FSM.

The accelerometer-assisted tracking is compared to the case using optical tracking only in Figure 13b under a vibration signal of 45 Hz. It is seen that reducing the optical tracking update rate and 'assisting' with accelerometer information (for four intermediate frames) yields very good tracking of the vibrating beacon signal. This same experiment was repeated for various vibration signals. Under the influence of these vibration signals, the results indicate that, on average, the FPA update rate can be reduced by a factor of 5 when maintaining the centroid accuracy to 1/10th pixel. The tracking was very good even with a distorted sinusoid vibration signal (caused by the vibration platform). The transmit and beacon signals show a time delay that is due to integration, centroid computation, image transfer and mirror update existing in the legacy hardware. This has been previously quantified to be 1.5-3 samples [10], depending on frame rate.

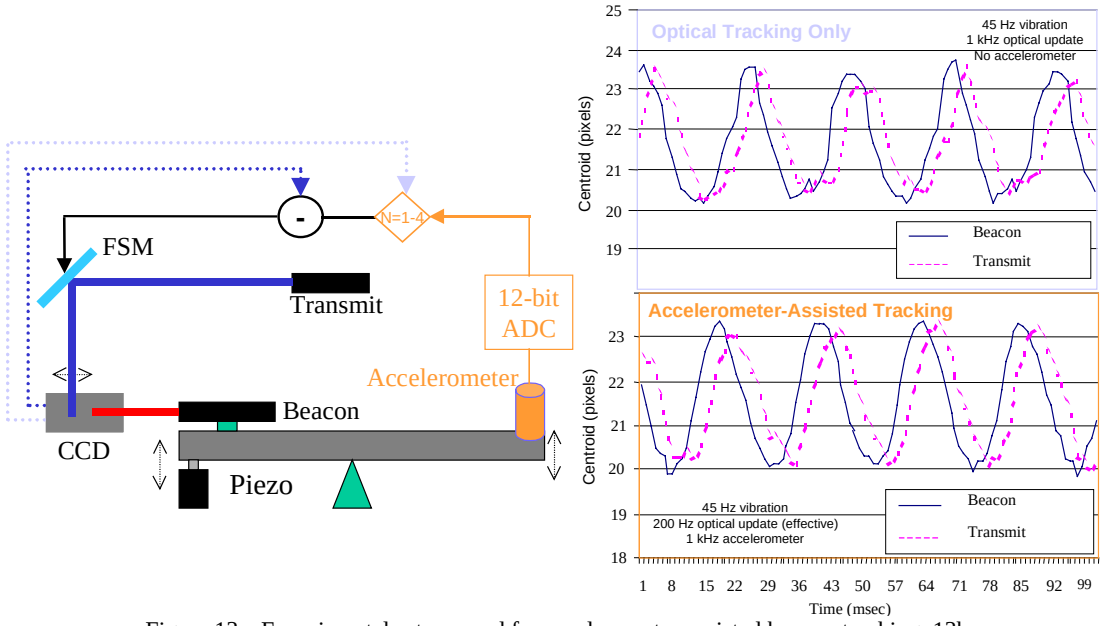

Figure 13a. Experimental set-up used for accelerometer-assisted beacon tracking. 13b. Accelerometer-assisted tracking

5 CONCLUSION

This article covered innovative hardware, algorithms, and architectures, techniques and recent laboratory results that are applicable to all deep space optical communication links, such as the Mars Telecommunication Network.

In particular this article presented the architecture of the sub-microradian pointing system for deep space optical communications with the analysis of the various pointing errors. The new pointing system architecture would allow stable pointing operations even under low intensity reference sources by employing inertial sensors, which is critical for deep space missions where the high intensity optical reference sources are not readily available. This inertial sensor (accelerometer) tracking approach promises the improvements of the performance of ATP subsystem while using the low intensity beacon sources such as uplink laser, stars, and Sun-illuminated Earth images as optical references. The primary challenge in using accelerometers to achieve the desired tracking performance is the minimization of the total random noise in acceleration measurements. Future work includes upgrades of hardware to lower the random noise.

Progress in the development of advanced hardware and algorithms was also presented. Including a versatile ATP Testbed, an improved rejection bandwidth pointing controller, a high-frame rate camera, and a vibration platform testbed.

Lastly, a laboratory demonstration of accelerometer-assisted beacon tracking was presented. By interlacing a fast-rate control loop (based on an inertial sensor) with a slow-rate control loop (optical tracking) a novel architecture has been validated. This novel architecture presents significant possibilities for deep space optical communications. This new architecture is not limited in range because the optical tracking reference can be supplied by laser beacon, star trackers or extended earth-image. It also no longer requires a high-speed FPA for receiver location updates. It inserts an 'estimator' to make use of inertial measurements as well as optical measurements. Furthermore, this new architecture is capable of removing the intrinsic time delay (image exposure duration) with high bandwidth inertial sensor; it makes the mirror control error independent of optical frame rate; it makes the ATP sub-system independent of particular sensors; and can still be used in an optical-only system.

6 ACKNOWLEDGEMENT

The authors wish to thank Steve P. Monacos, Angel A. Portillo, Bill Liu, Caroline Racho, Christian Jeppesen and Juan Ceniceros for their invaluable support and contributions to this work.

The work described was funded by the Cross-Enterprise Technology Development Program and performed at the Jet Propulsion Laboratory, California Institute of Technology under contract with the National Aeronautics and Space Administration.

Reference herein to any specific commercial product, process, or service by trade name, trademark, manufacturer, or otherwise, does not constitute or imply its endorsement by the United States Government or the Jet Propulsion Laboratory, California Institute of Technology.

7 REFERENCES

[1] S. Lee, J. W. Alexander and G. G. Ortiz, "Sub-microradian pointing system design for deep-space optical communications," in *Free-Space Laser Communication Technologies XIII*, G. Stephen Mecherle, Editor, Proceedings of the SPIE Vol. 4272, pp. TBD (2001).

[2] M. Jeganathan, A. Portillo, C. Racho and S. Lee, "Lessons learnt from the Optical Communications Demonstrator (OCD)," in *Free-Space Laser Communication Technologies XI*, G. Stephen Mecherle, Editor, Proceedings of the SPIE Vol. 3615, pp. 23-30 (1999).

[3] D. Russell, H. Ansari, C.-C. Chen, "Lasercom pointing, acquisition and tracking control using a CCD-based tracker," in *Free-Space Laser Communication Technologies VI*, G. Stephen Mecherle, Editor, Proceedings of the SPIE Vol. 2123, pp. 294-303 (1994).

[4] J. W. Alexander, S. Lee and C.-C. Chen, "Pointing and tracking concepts for deep space missions," in *Free-Space Laser Communication Technologies XI*, G. Stephen Mecherle, Editor, Proceedings of the SPIE Vol. 3615, pp. 230-249 (1999).

[5] Michael F. Luniewicz, Jerold P. Gilmore, Tze Thong Chien, and James E. Negro, "Comparison of wide-band inertial line of sight stabilization reference mechanizations", *Proceedings of SPIE International Symposium on Aerospace/Defense Sensing* (Conference 1697) – *Acquisition, Tracking, and Pointing* VI, pp.378-398, 1992.

[6] Dan Eckelkamp-Baker, Henry R. Sebesta, and Kevin burkhard, "Maghetohydrodynamic Inertial Reference System", *Acquisition, Tracking, and Pointing, Proceedings of SPIE*, Vol.4025, pp.99-110, 2000.

[7] C.-C. Chen, J. W. Alexander, H. Hemmati, S. Monacos, T. Y. Yan, S. Lee, J.R. Lesh, and S. Zingles, "System requirements for a deep-space optical transceiver", *Free-Space Laser Communication Technologies* XI, *Proc. SPIE*, Vol.3615, 1999.

[8] A. Portillo, G. G. Ortiz, C. Racho, "Fine Pointing Control for Optical Communications," in *IEEE Aerospace Conference*, Big Sky, Montana, Vol. TBD, pp. TBD (2001).

[9] B. Lurie, "Feedback limits in the steering mirror loops caused by computer delay", *JPL Internal Memorandum*, September 2000.

[10] C. Racho and A. Portillo, "Characterization and design of digital pointing subsystem for optical communication demonstrator," in *Free-Space Laser Communication Technologies XI*, G. Stephen Mecherle, Editor, Proceedings of the SPIE Vol. 3615, pp. 250-261 (1999).

[11] S. P. Monacos, A. A. Portillo, W. Liu, J. W. Alexander, and G. G. Ortiz, "A High-Frame Rate CCD Camera with Region-of-Interest Capability," in *IEEE Aerospace Conference*, Big Sky, Montana, Vol. TBD, pp. TBD (2001).

[12] Texas Instruments, "680x500 Pixel CCD Image Sensor TC237", June 1996.

[13] Texas Instruments, "3-V 10-Bit 27 MSPS Area CCD Sensor Signal Processor TLV987", September 1999.

[14] G. G. Ortiz, A. Portillo, S. Lee, and Juan Ceniceros, "Functional demonstration of accelerometer-assisted beacon tracking," in *Free-Space Laser Communication Technologies XIII*, G. Stephen Mecherle, Editor, Proceedings of the SPIE Vol. 4272, pp. TBD (2001).

[15] S. Lee, J. W. Alexander, G. G. Ortiz and C.-C. Chen, "Accelerometer-assisted tracking for free-space optical communications," in *JPL Optical Communications Group Progress Report*, Vol. 2000, No. 1, pp. 1-28 (2000).

[16] Juan Ceniceros, C. Jeppesen and G. G. Ortiz, "Vibration platform testbed for deep-space acquisition, tracking and pointing," in *Free-Space Laser Communication Technologies XIII*, G. Stephen Mecherle, Editor, Proceedings of the SPIE Vol. 4272, pp. TBD (2001).

[17] S. Lee, G. G. Ortiz, J. W. Alexander, A. Portillo, C. Jeppesen, "Accelerometer-assisted tracking and pointing for deep-space optical communications: concept, analysis, and implementations," in *IEEE Aerospace Conference*, Big Sky, Montana, Vol. TBD, pp. TBD (2001).

[18] M. Jeganathan and S. Monacos, "Performance analysis and electronics packaging of the Optical Communications Demonstrator," in *Free-Space Laser Communication Technologies X*, G. Stephen Mecherle, Editor, Proceedings of the SPIE Vol. 3266, pp. 33-40 (1998).